Monolithic integration of electroabsorption modulators and tunnel injection distributed feedback lasers using quantum well intermixing*

Wang Yang(汪 洋)†, Pan Jiao-Qing(潘教青), Zhao Ling-Juan(赵玲娟), Zhu Hong-Liang(朱洪亮), and Wang Wei(王 圩)

Key Laboratory of Semiconductor Materials Science, Institute of Semiconductors, Chinese Academy of Sciences, P. O. Box 912, *Beijing* 100083, *China*

(Received 2 June 2010; revised manuscript received 22 June 2010)

Electroabsorption modulators combining Franz–Keldysh effect and quantum confined Stark effect have been monolithically integrated with tunnel-injection quantum-well distributed feedback lasers using a quantum well intermixing method. Superior characteristics such as extinction ratio and temperature insensitivity have been demonstrated at wide temperature ranges.

Keywords: electroabsorption modulator, tunnel injection, wide temperature range operation, quantum well intermixing

PACC: 4280S, 4282

1. Introduction

Electroabsorption modulated lasers (EMLs) have been widely used in high speed fibre optical communications as the light sources. In such EMLs, electroabsorption modulators (EAMs) are monolithically integrated with distributed feedback (DFB) lasers. The output light power can be modulated in the EAMs utilizing the Franz–Keldysh effect (F-KE) or the quantum confined Stark effect (QCSE).[1−10] Wide temperature operation is desired to lower the power consumption with the demand of EMLs increasing. The uncooled operations of 1.55-μm 10-Gb/s and 40-Gb/s EMLs have been realized in InGaAlAs-InP material systems due to large conduction band offset ($\Delta E_{\rm c}$) and small valence band offset ($\Delta E_{\rm v}$) between quantum wells (QW) and barriers.[8,11−16] However, conventional InGaAsP-InP DFB lasers cannot work at high temperatures easily and show a lower characteristic temperature (T_0) than that of InGaAlAs-InP system because of the poor electron confinement in quantum wells with small $\Delta E_{\rm c}$. To overcome the disadvantage of small $\Delta E_{\rm c}$ and make InGaAsP-InP EMLs operate in a wide temperature range, a tunnel injection (TI) quantum well scheme was proposed.[17,18]

As shown in Fig. 1, electron currents are analysed in InGaAlAs quantum well (Fig. 1(a)), InGaAsP quantum well (Fig. 1(b)), and InGaAsP tunnel injection quantum well (Fig. 1(c)). In Figs. 1(a) and 1(b), the injection electron currents ($I_{\rm in}$) are separated into two parts, the current due to captive electrons in QW ($I_{\rm cap}$) and the current due to leakage electrons ($I_{\rm leak}$). The energy of partial captive electrons in QW transfers to photons through radiative transition ($I_{\rm rad}$), while another part of these captive electrons recombine with holes without radiation ($I_{\rm non-rad}$) such as Auger recombination. The leakage current and the nonradiative current are the main causes for the degeneration of laser diodes at high operation temperatures. Owing to larger $\Delta E_{\rm c}$, InGaAlAs-QW is able to confine electrons better than InGaAsP-QW, and $I_{\rm leak}$ is smaller in InGaAlAs-QW. In Fig. 1(c), the electrons are firstly thermalized in a narrow bandgap (slightly bigger than QW) bulk material, namely injector layer and then directly injected in QW through tunneling a thin and high barrier, which blocks hot carriers and makes $I_{\rm leak}$ small. The tunnel injection quantum well lasers with good performance have been realized, exhibiting the wide temperature operation capability.[18−20]

*Project supported by the National Natural Science Foundation of China (Grant Nos. 60736036, 60706009, 60777021 and 60702006), the National Basic Research Program of China (Grant Nos. 2006CB604901 and 2006CB604902), and the National High Technology Research and Development Program of China (Grant Nos. 2007AA03Z419, 2007AA03Z417 and 2009AA03Z442).

†Corresponding author. E-mail: wangyang06@semi.ac.cn

© 2010 Chinese Physical Society and IOP Publishing Ltd

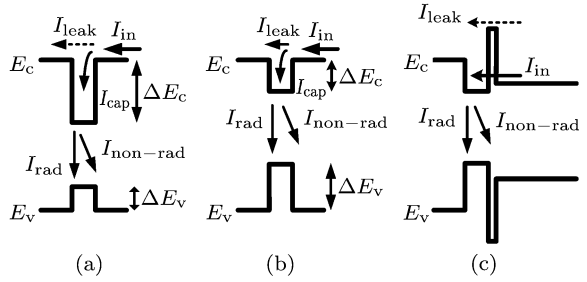


Fig. 1. Electron currents in (a) InGaAlAs quantum well, (b) InGaAsP quantum well and (c) InGaAsP tunnel injection quantum well.

In addition to power consumption, the fabrication cost is another problem of wide application. Easy fabrication processes are preferable on condition that device performance is acceptable. There have been many methods to obtain photonic integrated circuits (PICs), such as butt-joint method,[4,5] selective area growth (SAG) method,[1,6,10] twin waveguide method[7,8] and identical active layer (IAL) method,[9] an especial method for EML fabrication. However, these methods have their own drawbacks. For example, butt-joint method involves a selective etching and a regrowth of active layer, which requires rigorous control. For the SAG method, the undesired thickness change between the selective growth area and planar growth area depresses optical confinement and coupling. The IAL is an easy and low-cost method, using detuning between Bragg wavelength and gain/absorption peak wavelength, but sacrifices the gain of laser and the insertion loss of modulator. As a substitute for the IAL method, an ion-implantation-induced quantum-well-intermixing (QWI) process is employed in this work, which preserves optical gain in un-implanted section and forms blue shift of band edge in implanted section after annealing.[21] Owing to the TI structure, the EAMs in our design combine QCSE in disordered QWs with F-KE in the injector layer, compared with conventional quantum well structures using only QCSE as shown in Fig. 2.[22,23]

In Figs. 2(a) and 2(c), the bandgap energy of QW (ΔE_{g1}) is larger than the photon energy ($h\nu$) and photons can hardly be absorbed by QW. The bandgap of QW (ΔE_{g2}) under electric field becomes smaller and photons can easily be absorbed using QCSE in both Figs. 2(b) and 2(d). In addition to absorption in QW, figure 2(d) shows that the injector layer in TI-QW makes a contribution to photon absorption using F-KE, which is beneficial to the improvement of extinction characteristic of disordered QW.

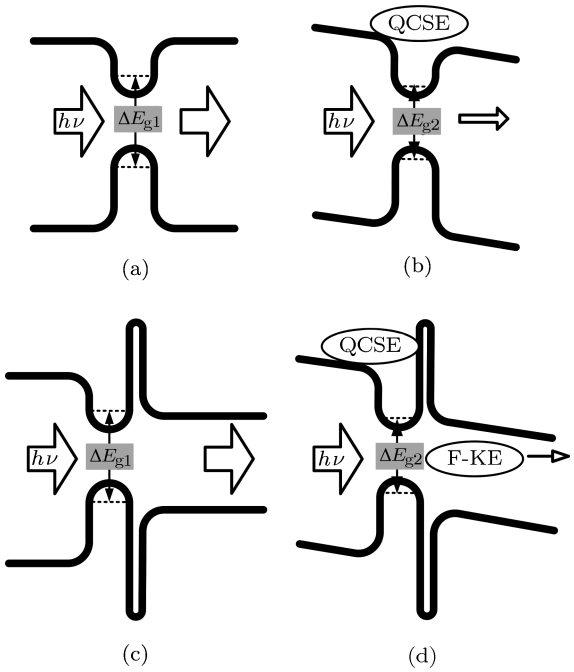


Fig. 2. Schematic band diagrams of conventional QW without (a) and with (b) reverse bias and tunnel-injection QW without (c) and with (d) reverse bias.

In this paper, tunnel-injection quantum-well (TI-QW) DFB lasers are used to achieve wide temperature range operation of EMLs for the first time, and low-cost QWI process is utilized to obtain the blue shift of bandgap in EAM, in which F-KE is combined with QCSE.

2. Device fabrication

The structure grown on a sulfur-doped InP substrate by metal–organic chemical vapour deposition (MOCVD) is shown in Fig. 3.

InP implant buffer layer	2500 Å
1.2Q SCH layer	1000 Å
8 QWs	8 × (57 Å+140 Å)
InP injection barrier layer	30 Å
1.47Q injector layer	500 Å
1.2Q SCH layer	500 Å
n-InP buffer	
n-InP substrate	

Fig. 3. Epitaxy structure prior to QWI by MOCVD (1 Å=0.1 nm).

In conventional MQW laser structure, QWs are sandwiched by separate confinement heterostructure (SCH) layers. In contrast, a 500-Å lattice matching InGaAsP layer with a photoluminescence (PL) peak at 1.47 μm and a 30-Å InP tunnel barrier were grown followed by the first quantum well in the TI-QW structure. Eight 57-Å compressively strained (1.57%) quantum wells and 140-Å tensile strained (0.4%) barriers were grown alternately before a 1000-Å SCH layer. Afterwards, the basic TI-QW structure was covered by a 2500-Å InP implanting buffer.

The laser regions were masked with 4500-Å SiO_2 layer, and P^+ ions were implanted in the EAM regions with an energy of 30 keV and a dose of 5×10^{13} cm^{-2} at a substrate temperature of 200 °C. The projected range of the implanted P^+ ions in InP layer was only 360 Å, creating no damage in the active region. Then a 240-second, 650 °C rapid thermal anneal (RTA) was carried out to diffuse the vacancies through quantum well structure and intermix the components of adjacent quantum wells and barriers, resulting in blue shift of the EAM region. As shown in Fig. 4, the PL peak of EAM ($\lambda_{\rm EAM}$) after RTA was shifted by 58 nm relative to the laser section.

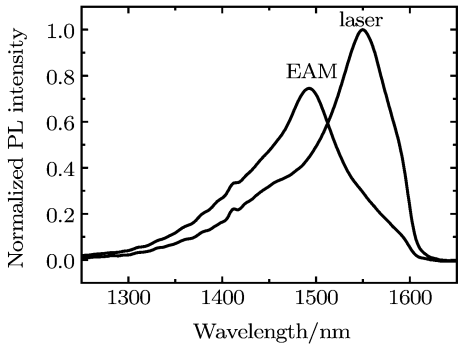


Fig. 4. Normalized PL spectra of laser and EAM sections after RTA.

After removing the InP implant buffer, holographic grating with a period of 242 nm was etched on the upper SCH layer in the laser section. Following a regrowth of InP layer to bury the grating, a 200-Å InGaAsP etching stop layer, a 17000-Å p-InP cladding layer and a 2000-Å p^+-InGaAs contact layer were grown in sequence.

A conventional 3-μm-width ridge waveguide structure was formed by dry and wet etching. The top contact layer of a 50-μm-long isolation section between DFB laser and EAM was removed and He^+ implantation was used to increase the isolation resistance. Then the surface of the wafer was covered by a 4000-Å SiO_2 passivation layer with contact layers on the top of DFB and EAM sections exposed. Eventually, the p- and n-electrodes were made. The final device structure was shown in Fig. 5, and total length of the device is 470 μm, including a 250-μm DFB laser and a 170-μm EAM.

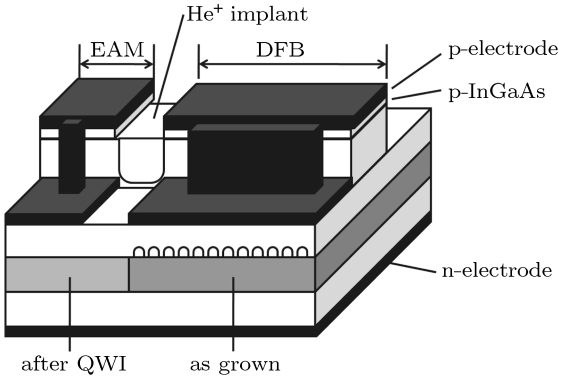


Fig. 5. Schematic structure of final devices.

3. Structure analysis

The conductive band offset between quantum well and barrier in our structure is 89 meV, while $\Delta E_{\rm c}$ between 1.47Q injector layer and InP injection barrier is over 200 meV. The relationship between leakage current and $\Delta E_{\rm c}$ is given by

$$I_{\rm leak} \sim \exp\left[\left(E_{\rm fc} - \Delta E_{\rm c}\right)/k_{\rm B}T\right], \tag{1}$$

where $E_{\rm fc}$ is the Fermi level of conductive band, $k_{\rm B}$ is the Boltzmann constant, and T is the absolute temperature. So at room temperature, leakage current through InP injection barrier in the TI-QW structure is about 1.4% of that through 1.2Q barrier in conventional QW structure.

The fundamental transverse mode of the ridge waveguide is calculated by beam propagation method, in which the multiple-quantum-well region is treated as a bulk material with an efficient refractive index

$$N_{\rm eff} = \sqrt{\left(t_{\rm w} \cdot N_{\rm w}^2 + t_{\rm b} \cdot N_{\rm b}^2\right)/\left(t_{\rm w} + t_{\rm b}\right)}, \tag{2}$$

where $t_{\rm w}/t_{\rm b}$ and $N_{\rm w}/N_{\rm b}$ are thickness and refractive index of a quantum well/barrier respectively. Optical mode profile $U(y)$ around the active region in the vertical (y) direction is depicted in Fig. 6.

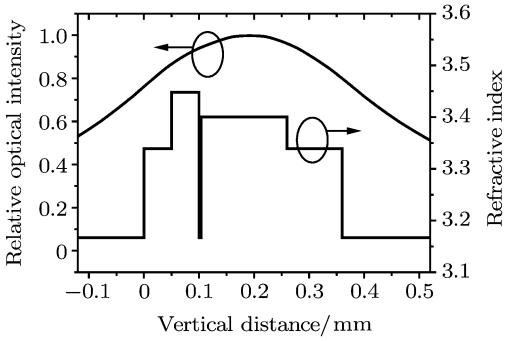


Fig. 6. Calculated optical mode profile and refractive index distribution in vertical direction.

The optical confinement factor in the multiple-quantum-well region (Γ_{MQW}) of 30.176% can be obtained as

$$\Gamma_{\mathrm{MQW}} = \frac{\int_{0.1030}^{0.2606} U(y)\mathrm{d}y}{\int_{-\infty}^{\infty} U(y)\mathrm{d}y}, \tag{3}$$

while that in the injector layer (Γ_{IL}) of 11.341% is similarly calculated from

$$\Gamma_{\mathrm{IL}} = \frac{\int_{0.05}^{0.1} U(y)\mathrm{d}y}{\int_{-\infty}^{\infty} U(y)]\mathrm{d}y}. \tag{4}$$

As the introduction of a high-refractive-index injector layer close to multiple-quantum-well region, the Γ_{MQW} is slightly higher than that of conventional QW structure with 100-nm-thick upper and lower SCH layers, thereby improving the mode gain of laser.

The absorption of TI-QW in an electric field can be divided into two parts: utilizing QCSE in QWs and F-KE in injector layer. $\Delta\alpha_{\mathrm{QCSE}}(E)$ and $\Delta\alpha_{\mathrm{F-KE}}(E)$ are defined as absorption coefficient changes in QW and injector layer with the electronic field E respectively, and static extinction ratio (ER) is given by

$$\mathrm{ER} = 10\log\left(\frac{P(E)}{P(0)}\right) \approx 10\log\left[\exp\left(-\Delta\alpha_{\mathrm{QCSE}}\frac{t_{\mathrm{w}}}{t_{\mathrm{w}}+t_{\mathrm{b}}}\Gamma_{\mathrm{MQW}}L - \Delta\alpha_{\mathrm{F-KE}}\Gamma_{\mathrm{IL}}L\right)\right], \tag{5}$$

where $P(E)/P(0)$ is the output power from EAM with/without bias electric field E, and L is the length of EAM. The first and second exponential terms on the right-hand side of Eq. (5) denote the absorptions in QWs and in injector layer respectively, while the second term was absent in the case of EMLs with conventional QW.

If a thicker 1.47Q injector layer is applied, the Γ_{MQW} will change little and Γ_{IL} will be larger, which can improve the ER characteristic. However, the bandgap of 1.47Q is so close to lasing photon energy that thicker injector layer lowers the mode gain in laser and increases the insertion loss in EAM. So a 50-nm-thick injector layer is chosen for the first experiment.

4. Experiment result

The TI-QW DFB lasers were cleaved into discrete devices, and light–current (L–I) curves at various temperatures were measured as shown in Fig. 7. A characteristic temperature of 70 K has been achieved, indicating wide temperature range operation of the lasers. A threshold current (I_{th}) of 23 mA and a slop efficiency of 0.19 mW/mA per facet are exhibited at 10 °C. The lasing wavelength ($\lambda_{\mathrm{lasing}}$) is around 1.57 μm, which is not sensitive to the temperature with a red shift of 0.1 nm/°C.

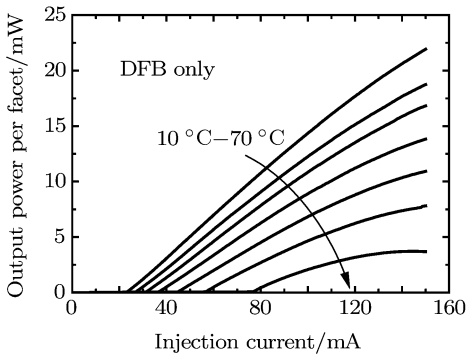


Fig. 7. Light–current curves of DFB lasers from 10 °C to 70 °C.

Figure 8 shows the curves for output power from EAM end versus the injection current to DFB laser of an integrated device under EAM voltage from 0 V to –5 V at 25 °C. The threshold current of the EML is 30 mA, which is nearly the same as that of discrete DFB lasers. The output power reaches up to 5 mW with a laser current less than 100 mA at 0 V EAM bias, showing a slop efficiency of 0.08 mW/mA. The isolation resistance between p-electrodes of EAM and DFB laser is as high as 200 kΩ, so a fixed I_{th} is

achieved at various EAM reverse biases.

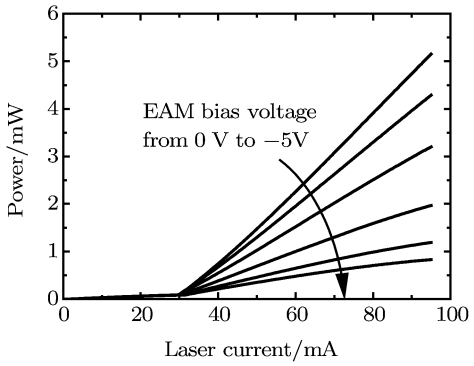


Fig. 8. *L–I* curves of an integrated device under various bias voltages of EAM.

Another EML chip with conventional QW structure was also fabricated using the QWI method, and wavelength detuning ($\Delta\lambda = \lambda_{\rm lasing} - \lambda_{\rm EAM}$) of $\sim$ 80 nm is the same as that of EML with TI-QW structure. The values of static extinction ratio have been measured by an integrating sphere, and superior characteristic of the TI-QW structure shown in Fig. 9 testifies the combination of F-KE and QCSE. And a comparatively small difference has been found between extinction ratios measured by an integrating sphere and a coupled single-mode fibre (over 10 dB at $V_{\rm pp} = 4$ V), which indicates a good optical coupling between DFB and EAM waveguides.

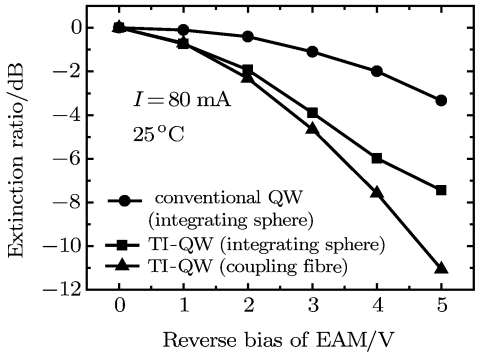


Fig. 9. Static extinction ratios of an EML with conventional quantum well structure and an EML with TI-QW structure.

The extinction characteristics at temperatures from 20 °C to 40 °C are shown in Fig. 10, and measured data are fitted to curves of third-order polynomials. It is found that the maximum extinction efficiency point of 4 V at 20 °C decreases to 3.5 V at 30 °C and 3 V at 40 °C, due to red shift of exciton absorption peak as temperature increases. On the other hand, the extinction efficiency decreases at higher temperatures because of the broadening of exciton absorption spectra. The two effects above are well compensated with each other in our devices, so the static extinction ratio varies very little with temperature, which makes possible the wide temperature range operation.

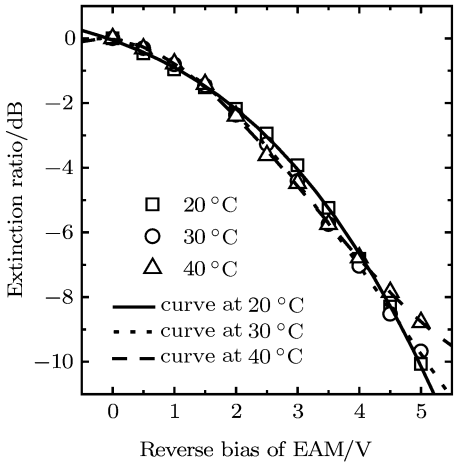


Fig. 10. Static extinction ratios at 20 °C, 30 °C, and 40 °C.

5. Conclusion

In this paper, an EAM has been monolithically integrated with a TI-QW DFB laser using the low-cost QWI method, based on the InGaAsP/InP material system. The integrated EML operating with a threshold current of 30 mA, a slop efficiency of 0.08 mW/mA and an extinction ratio over 10 dB at $V_{\rm pp}$ of 4 V has been demonstrated. The combination of F-KE and QCSE in EAM by the TI-QW structure shows favourable performances. The low sensitivity to operating temperature of extinction ratio proves the wide temperature rang operation potential of our devices.

References

[1] Ishizaka M, Yamaguchi M, Shimizu J and Komatsu K 1997 *IEEE Photon. Technol. Lett.* **9** 1628

[2] Suzuki M, Noda Y, Tanaka H, Akiba S, Kushiro Y and Isshiki H 1987 *J. Lightwave Technol.* **5** 1277

[3] Sahlen O 1994 *J. Lightwave Technol.* **12** 969

[4] Takeuchi H, Tsuzuki K, Sato K, Yamamoto M, Itaya Y, Sano A, Yoneyama M and Otsuji T 1997 *IEEE Journal of Selected Topics in Quantum Electronics* **3** 336

[5] Miyazaki Y, Tada H, Aoyagi T, Nishimura T and Mitsui Y 2002 *IEEE J. Quantum Electron.* **38** 1075

[6] Aoki M, Takahashi M, Suzuki M, Sano H, Uomi K, Kawano T and Takai A 1992 *IEEE Photon. Technol. Lett.* **4** 580

[7] Stegmueller B, Baur E and Kicherer M 2002 *IEEE Photon. Technol. Lett.* **14** 1647

[8] Kobayashi W, Tsuzuki K, Shibata Y, Yamanaka T, Kondo Y and Kano F 2009 *J. Lightwave Technol.* **27** 5084

[9] Delprat D, Ramdane A, Ougazzaden A, Nakajima H and Carre M 1997 *Electron. Lett.* **33** 53

[10] Zhao Q, Pan J Q, Zhang J, Li B X, Zhou F, Wang B J, Wang L F, Bian J, Zhao L J and Wang W 2006 *Acta Phys. Sin.* **55** 1259 (in Chinese)

[11] Saravanan B K, Wenger T, Hanke C, Gerlach P, Peschke M and Macaluso R 2006 *IEEE Photon. Technol. Lett.* **18** 862

[12] Aubin G, Seoane J, Merghem K, Berger M S, Jespersen C F, Garreau A, Blache F, Jany C, Provost J G, Kazmierski C and Jeppesen P 2009 *Electron. Lett.* **45** 1263-U100

[13] Kobayashi W, Arai M, Yamanaka T, Fujiwara N, Fujisawa T, Ishikawa M, Tsuzuki K, Shibata Y, Kondo Y and Kano F 2009 *IEEE Photon. Technol. Lett.* **21** 1054

[14] Kobayashi W, Yamanaka T, Arai M, Fujiwara N, Fujisawa T, Tsuzuki K, Ito T, Tadokoro T and Kano F 2009 *IEEE Photon. Technol. Lett.* **21** 1317

[15] Makino S, Shinoda K, Kitatani T, Hayashi H, Shiota T, Tanaka S, Aoki M, Sasada N and Naoe K 2009 *IEICE Transac. Electron.* **E92c** 937

[16] Kobayashi W, Arai M, Yamanaka T, Fujiwara N, Fujisawa T, Tadokoro T, Tsuzuki K, Kondo Y and Kano F 2010 *J. Lightwave Technol.* **28** 164

[17] Sun H C, Davis L, Lam Y, Sethi S, Singh J and Bhattacharya P K 1994 *Gallium Arsenide and Related Compounds 1993* **136** 197

[18] Bhattacharya P, Zhang X K, Yuan Y S, Kamath K, Klotzkin D, Caneau C and Bhat R 1998 *Physics and Simulation of Optoelectronic Devices* Vi, Parts 1 and 2 **3283** 702

[19] Bhattacharya P, Yuan Y, Brock T, Caneau C and Bhat R 1998 *IEEE Photon. Technol. Lett.* **10** 778

[20] Yoon H, Gutierrezaitken A L, Jambunathan R, Singh J and Bhattacharya P K 1995 *IEEE Photon. Technol. Lett.* **7** 974

[21] Marsh J H 1993 *Semicond. Sci. Technol.* **8** 1136

[22] Ramdane A, Krauz P, Rao E V K, Hamoudi A, Ougazzaden A, Robein D, Gloukhian A and Carre M 1995 *IEEE Photon. Technol. Lett.* **7** 1016

[23] Raring J W, Johansson L A, Skogen E J, Sysak M N, Poulsen H N, DenBaars S P and Coldren L A 2007 *J. Lightwave Technol.* **25** 239